Available online at www.sciencedirect.com

SciVerse ScienceDirect

Ceramics International 39 (2013) 1749–1755

CERAMICS INTERNATIONAL

www.elsevier.com/locate/ceramint

Room-temperature synthesis of CuO/graphene nanocomposite electrodes for high lithium storage capacity

Seung-Deok Seo, Duk-Hee Lee, Jae-Chan Kim, Gwang-Hee Lee, Dong-Wan Kim*

Department of Materials Science and Engineering, Ajou University, San 5, Woncheon-dong, Yeongtong-gu, Suwon 443-749, South Korea

Received 23 July 2012; received in revised form 7 August 2012; accepted 7 August 2012
Available online 18 August 2012

Abstract

A facile approach for the synthesis of hybrid nanocomposite electrodes comprising pine-nut-shaped cupric oxide (CuO) particles and electrolytically exfoliated conducting graphene nanosheets (GNSs) for lithium ion battery applications is demonstrated. The GNSs were initially dispersed in aqueous solution, and then, $Cu(OH)_2$ was synthesized by the reaction of $CuSO_4 \cdot 5H_2O$, NH_4OH, and NaOH. In the subsequent chemical reduction process, a controlled amount of hydrazine hydrate ($N_2H_4 \cdot H_2O$) was added to the reaction mixture to obtain the CuO/GNS nanocomposite. Information about the phase, surface properties, and morphology of the CuO and CuO/GNS composite was obtained by X-ray diffraction, Brunauer–Emmett–Teller surface analysis, field-emission scanning electron microscopy, and high-resolution transmission electron microcopy. The electrochemical performance of the nanocomposite was evaluated by cyclic voltammetry and galvanostatic cycling. The nanocomposite synthesized by this method had a uniform morphology without aggregation and showed enhanced electrochemical performances.

Keywords: Copper oxide; Graphene nanocomposites; Lithium ion batteries; Chemical reduction

1. Introduction

In recent years, high-performance lithium-ion batteries (LIBs) have found widespread applications in portable electronic devices such as mobile phones as well as in various kinds of electric vehicles. To date, graphite has been used as the conventional anode material in LIBs but its limited theoretical capacity (of 372 mA h g^{-1}) has inspired intensive research toward alternative anode materials [1].

Nanosized transition-metal oxides (M_xO_y; M: Cu, Co, Fe) are promising candidates for anode materials in LIBs, because the metal particles are lithium-inactive and can be easily dispersed in the Li_2O matrix; further, M_xO_y nanodomains would be formed during lithium insertion/desertion (conversion reaction) [2]. The monoclinic cupric oxide (CuO) also undergoes a conversion reaction with two lithium ions per mole ($CuO + 2Li^+ + 2e^- \leftrightarrow Cu + Li_2O$, 674 mA h g^{-1}) [3]. The various procedures adopted for the synthesis of nano-sized CuO anodes are thermal decomposition, thermal dehydration, electrochemical methods, thermal reduction, and the hydrothermal method [4–8].

In contrast to the graphite anode, which is well known for its advantages such as reversible capacity, low reaction potential, eco-friendliness, and low cost, CuO and other conversion anode materials (3d transition-metal oxides, fluorides, and phosphides) have critical drawbacks such as slow reaction kinetics resulting from the complexity of the conversion reaction [9]. Recently, to improve the kinetics and cycle life of anode materials, various strategies such as nanostructure diversification and composite formation with other conductive materials have been reported [10–13]. The most attractive method among these is composite formation with a conducting material such as a lithium-inactive metal or a carbonaceous material. It is known that the addition of a carbonaceous material effectively improves conductivity, prevents aggregation, and relaxes mechanical stress of the anode [14–16].

A graphene nanosheet (GNS) is one of advanced carbonaceous materials, which has single or few layers graphite (002) planes. It has high surface area, superior

*Corresponding author. Tel.: +82 31 219 2468; fax: +82 31 219 3248.
E-mail address: dwkim@ajou.ac.kr (D.-W. Kim).

0272-8842/$ - see front matter © 2012 Elsevier Ltd and Techna Group S.r.l. All rights reserved.
http://dx.doi.org/10.1016/j.ceramint.2012.08.021

conductivity, high porosity, and other fascinate properties. Because of abovementioned intrinsically charming properties, some researchers have been reported various composite nanostructures of CuO and graphene oxides, which shows enhanced lithium storage characteristics and cycle stabilities [17–19].

In this paper, we report a facile chemical reduction method for the synthesis of high-lithium-capacity pine-nut shaped CuO nanoparticles from a template-free $Cu(OH)_2$ nanowire precursor. The synthesis of a composite with electrolytically exfoliated graphene nanosheets is also shown. The CuO/GNS composite was prepared under the same conditions as those adopted for preparation of CuO, but a GNS-pre-dispersed aqueous solution was used. The synthesized powders were characterized for phase information, particle size, microstructure morphology, and GNS content by X-ray diffraction (XRD), field-emission scanning electron microscopy (FESEM), high-resolution transmission electron microcopy (HRTEM), Brunauer–Emmett–Teller (BET) surface analysis, and thermal gravimetric analysis (TGA). The electrochemical properties of each sample were evaluated by galvanostatic cycling and cyclic voltammetry.

2. Experimental details

2.1. Synthesis of CuO nanoparticles

CuO was synthesized by simple chemical reduction from $Cu(OH)_2$ nanowires. First, 30 ml of 0.15 M NH_4OH (28%–30% as ammonia) was added to 0.0064 M $CuSO_4 \cdot 5H_2O$ aqueous solution, and the resulting solution was stirred for 20 min. Then, 10 ml of 1.2 M NaOH solution was added to the abovementioned mixture and stirred in a similar manner as in the previous step. After the addition of OH^- sources and stirring for 20 min, the solution turned opaque and light blue in color, indicating the formation of $Cu(OH)_2$ nanowires. For reduction of the $Cu(OH)_2$ precursor, 2 ml of 1 M $N_2H_4 \cdot H_2O$ aqueous solution was added. After 4 h of constant stirring, the color of the solution became brown.

2.2. Synthesis of CuO/GNS nanocomposites

GNSs were prepared from graphite sheets by a simple electrochemical exfoliation route. The detailed description of the GNS synthesis has been included in our previous report [20]. The CuO/GNS synthesis method has one additional step in comparison with the CuO nanoparticle synthesis method. To obtain a uniform CuO/GNS composite, the as-prepared GNSs were dispersed in DI water for several hours before the addition of Cu sources; an ultrasonic generator (VCX 500, Sonics & Materials, Inc.) was used for the dispersion. The subsequent synthesis procedure is identical to the CuO synthesis. The obtained powders were washed and centrifuged several times with DI water and ethanol and then dried for 8 h at 80 °C in vacuum.

2.3. Material characterization

The crystal structure and morphology of each powder were analyzed by XRD (Miniflex II, Rigaku), FESEM (JSM-6330F, JEOL), and HRTEM (JEM-2100F, JEOL). The weight ratio and surface area of the CuO and CuO/GNS samples were obtained from TGA (DTG-60A, Shimadzu) and BET surface area analysis (Belsorp-mini II, BEL Japan).

2.4. Electrochemical measurements

The electrochemical performance of the CuO nanoparticles and CuO/GNS nanocomposite was evaluated using Swagelok-type half-cells. The cell was assembled in a glove box filled with high-purity Ar gas, and the as-prepared powders were stored in a convection oven maintained at 120 °C. A test electrode was prepared by depositing 1–2 mg of the active material on a 25-μm-thick Cu foil (Sigma-Aldrich) by a slip-casting method. The slurry was prepared by dispersing the active material (CuO, CuO/GNS), Super P carbon black (MMM carbon), and Kynar 2801 binder (PVDF-HFP) in 70:15:15 weight ratio in 1-methyl-2-pyrrolidinone (NMP, Sigma-Aldrich). The slurry-coated Cu foil electrode was baked in a vacuum oven at 100 °C for 4 h and used as the cathode in the half-cell, while a lithium foil was used as the anode. A separator film of Celgard 2400 and liquid electrolyte (EC: DMC, 1:1 by volume with 1.0 M $LiPF_6$) were also used. The assembled cells were galvanostatically cycled at a cutoff voltage of 0.01–3 V and various current rates using an automatic battery cycler (WBCS 3000, Wonatech). Cyclic voltammetry measurements at a scan rate of 0.3 mVS^{-1} were also carried out for the investigation of the chemical reaction with lithium.

3. Result and discussion

The synthesized CuO powder was analyzed by FESEM and XRD for obtaining morphology and phase information. The FESEM image of the CuO powder is shown in Fig. 1a. Most of the particles in the powder resembled pine-nut-like ellipsoids. From the FESEM image, it was clear that the nanoparticles had a uniform size distribution of about 200–300 nm in height and 100–150 nm in width. Moreover, each particle seemed to have a bumpy surface (see inset in Fig. 1a), i.e., each particle had a large surface area. BET measurements also revealed that the CuO nanoparticles had relatively a large surface area of over 30 $m^2 g^{-1}$, because of which a greater number of sites for reaction with lithium cations were available, resulting in better electrochemical properties. Some researchers correlated the electrochemical performance with the nanoparticle surface area and concluded that a large surface area allows for fast kinetics and better surface wetting of the electrolyte [21–22]. Moreover, the mechanism of CuO synthesis could be deduced from the microstructural

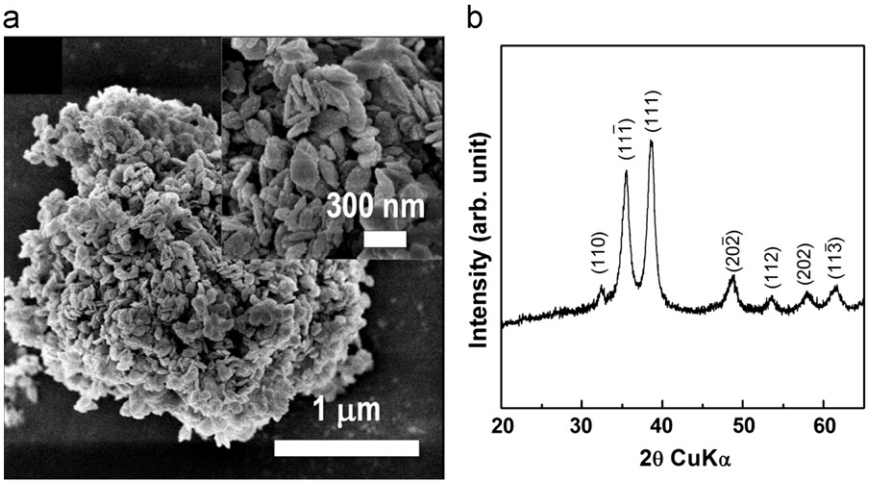

Fig. 1. (a) FESEM image of CuO nanoparticles (inset: magnified view). (b) Powder X-ray diffraction pattern of CuO nanoparticles.

information. The copper hydroxide precursor has a 1D nanowire structure, which is not stable in aqueous medium. Because of this instability, H_2O is released upon heating, thus inducing breakdown of the structure and reassembling in a single preferential direction. In our experiments, hydrazine hydrate ($N_2H_4 \cdot H_2O$) was used for reduction; the corresponding decomposition reaction is as follows:

$$NH_2NH_2 + H_2O \rightarrow NH_2NH_3 + OH^-$$

In aqueous solutions with high OH^- concentration (high pH), the solid $Cu(OH)_2$ can be dissolved by the excess OH^- anions in the solution. Consequently, the $[Cu(OH)_4]^{2-}$ complex formed acts as a precursor that transforms into crystalline CuO. Subsequently, the precipitated CuO particles fuse to yield a specific phase, thereby forming leaf-shaped particles. Cudennec and Lecerf [23] reported in detail about this topotactic transformation from $Cu(OH)_2$ to CuO, which can be expressed by the following reaction

$$Cu(OH)_2(s) + 2OH^-(aq) \rightarrow Cu(OH_4)^{2-}(aq)$$

$$Cu(OH)_4^{2-}(aq) \leftrightarrow CuO(s)$$

From the abovementioned data, we could understand the role of hydrazine in the CuO nanoparticle synthesis and the factor affecting the formation of the bumpy surface morphology. Fig. 1b shows the powder XRD pattern of the CuO nanoparticles. As shown in the diffraction patterns, synthesized CuO nanoparticles gave two sharp high-intensity peaks at 35.5° and 38.5°, which corresponded to the (11$\bar{1}$) and (111) planes, respectively. These data were in good agreement with the reference crystallographic data (JCPDS #48-1548) of monoclinic CuO. No peak due to the precursor $Cu(OH)_2$ was seen. Therefore, it was apparent that the crystalline $Cu(OH)_2$ was completely transformed into CuO by the aforementioned mechanism (which could also be a dehydration mechanism). Previously, Xiang et al. [24] reported that the morphology of the precipitated CuO could be affected by pH, which is controlled by the amount of ammonia, and discussed the effects of excess NH_4^+ cations in solution. Moreover, some researchers synthesized various CuO nanostructures by dehydration of the $Cu(OH)_2$ precursor, i.e., by heating the precursor in suspension or powder form. In contrast, our experiments were performed at room temperature by a simple, rapid, and facile chemical reduction route. The room-temperature synthesis is often preferred because heating might trigger growth and aggregation of the synthesized CuO. As mentioned above, anodes fabricated from transition-metal oxides have some undesirable drawbacks such as slow lithium-reaction kinetics caused by the complexity of the reaction. To overcome this problem and ensure better electrochemical performance, we prepared a CuO/GNS composite by a similar method. It is known that GNSs can be used as anode materials because they provide an efficient electron conduction pathway; further, when using GNSs, aggregation of the active particles is prevented, and a larger surface area that allows for better contact between the electrolyte and the active materials is obtained [25].

Fig. 2a shows the FESEM image of the CuO/GNS composite. The CuO nanoparticles have almost the same morphology as does pure CuO and are well dispersed on each GNS particle. The precipitation of a large number of crystalline CuO particles with uniform size distribution on the GNS surface was also confirmed in a typical HRTEM image (Fig. 2b and inset). To investigate the presence and amount of GNS, we performed powder XRD and TGA experiments on the prepared samples (Fig. 2c and d). The only notable difference between the XRD patterns of the pure CuO nanoparticles (Fig. 1b) and CuO/GNS nanocomposite (Fig. 2c), was the existence of a peak at around 25°, which was attributable to the presence of the GNS (002) planes, in the case of the composite. This observation confirmed the formation of the CuO/GNS composite.

Fig. 2d shows the precise affirmation of the weight ratio of the GNS and CuO in the composite. Both the TGA curves showed the same behavior in the temperature range

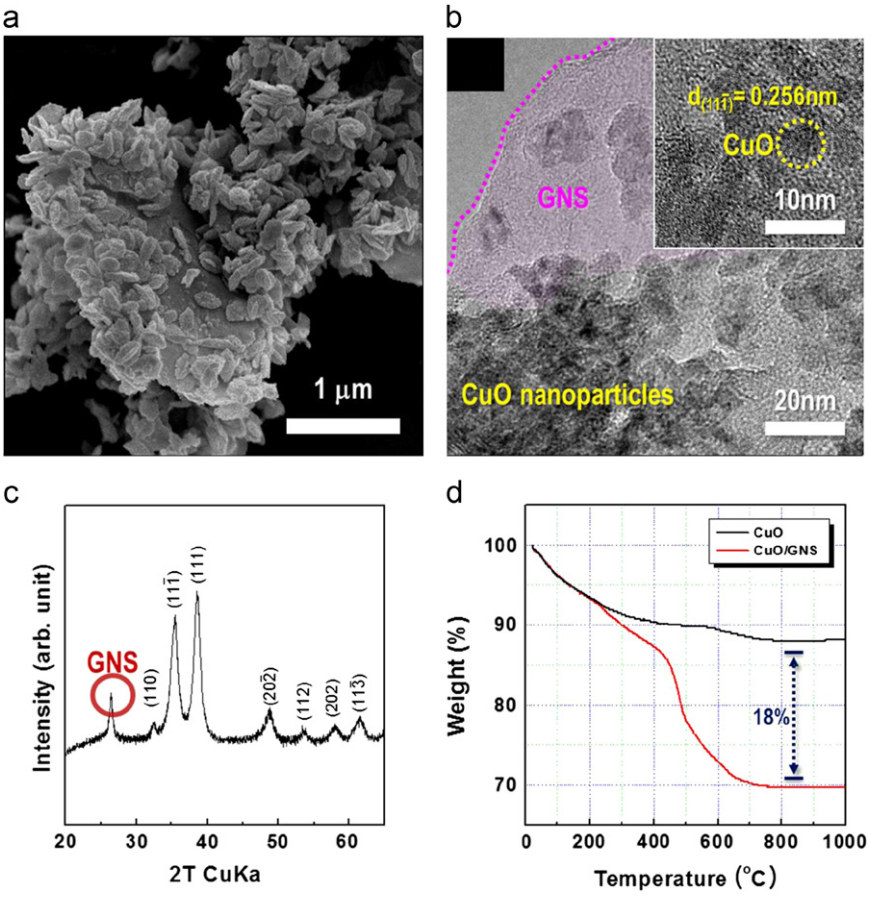

Fig. 2. (a) Typical FESEM image, (b) HRTEM image, and (c) XRD pattern of as-prepared CuO/GNS composite, respectively. Inset in (b) shows the formation of crystalline CuO on the GNS. (d) TGA curves of both CuO and CuO/GNS composite.

0–250 °C; from 400 °C, the weight percentage for the CuO/GNS composite (red curve) decreased drastically upto 800 °C and then remained constant till 1000 °C. This was because of the decomposition of the GNS (carbon) upon exposure to air. At 1000 °C, the weight difference between the samples was about 18%, which indicated the amount of GNS. For the electrochemical evaluations of the composites, the theoretical capacity of the CuO/GNS composite was calculated in accordance with the CuO:GNS (82:18 wt%) weight ratio because the GNSs may react with lithium. The calculated theoretical capacity of CuO/GNS (612.23 mA h g^{-1}), which was lower than that of pure CuO (674 mA h g^{-1}), was used to calculate the applied current in galvanostatic analysis.

The result of the cyclic voltammetry analysis of pure CuO and CuO/GNS is shown in Fig. 3a and b. The tests were performed in the voltage window 3.0–0.01 V at a scan rate of 0.3 mV s^{-1}. Pure CuO (Fig. 3a) showed three cathodic peaks (red line) at 1.94 V, 0.94 V, and 0.72 V with a negative sweep and an anodic peak at 2.5 V with a positive sweep. The cathodic and anodic peaks corresponded to lithium assimilation and release, respectively. The transformation $CuO \rightarrow Cu_2O \rightarrow Cu$ takes place in the cathodic process, and Li^+ cations escape from the CuO matrix [26]. In the subsequent cycles, the peaks became smaller but sharper. In the anodic scan, where lithium is released from the $Cu + Li_2O$ matrix, the anodic peak decreased in size upon repetitive cycling and became very small after 10 cycles. In contrast, the cyclic voltammogram of the CuO/GNS composite (Fig. 3b) showed the some similar features to those for pure CuO. In the cathodic reaction, three peaks at 1.5 V, 0.9 V, and 0.7 V appeared in the first cycle (red line). The first and third cathodic peaks appeared at a relatively lower voltage than that for the pure CuO electrode. After 10 cycles, the peaks did not show any significant change in position and intensity. A special feature in the case of the CuO/GNS electrode was the presence of an extra peak at a very low voltage of around 0.01 V. The shift of the anodic/cathodic peaks toward the low-voltage region was due to formation/deformation of a gel-like film, which resulted from the decomposition of the electrolyte [27].

Galvanostatic cycling was performed in the voltage window 3.0–0.01 V at a current rate of 0.2C. Fig. 4a shows the first 10 charge-discharge cycles of CuO and CuO/GNS composite. Although almost same voltage plateaus and sloped behaviors was observed in charge-discharge curves of both electrodes, the specific capacity of CuO/GNS composite is much higher than CuO nanoparticles. The cycling performance of CuO and CuO/GNS at 0.2C is also

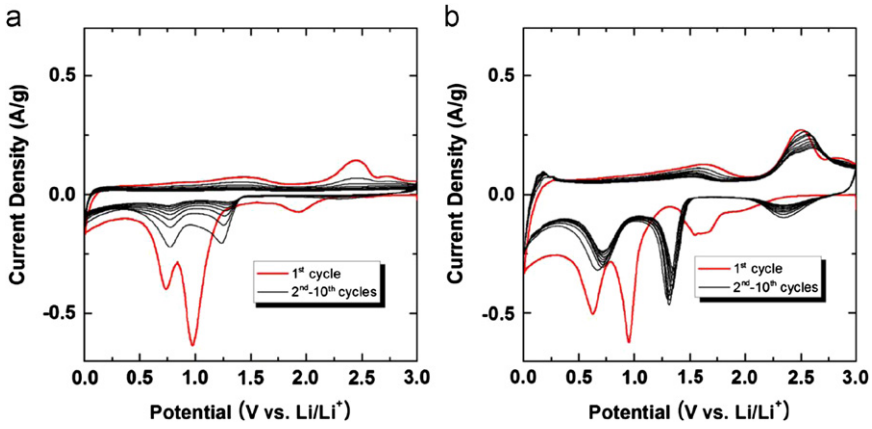

Fig. 3. Cyclic voltammograms of (a) pure pine-nut-shaped CuO and (b) CuO/GNS nanocomposite in the voltage range 3.0–0.01 V.

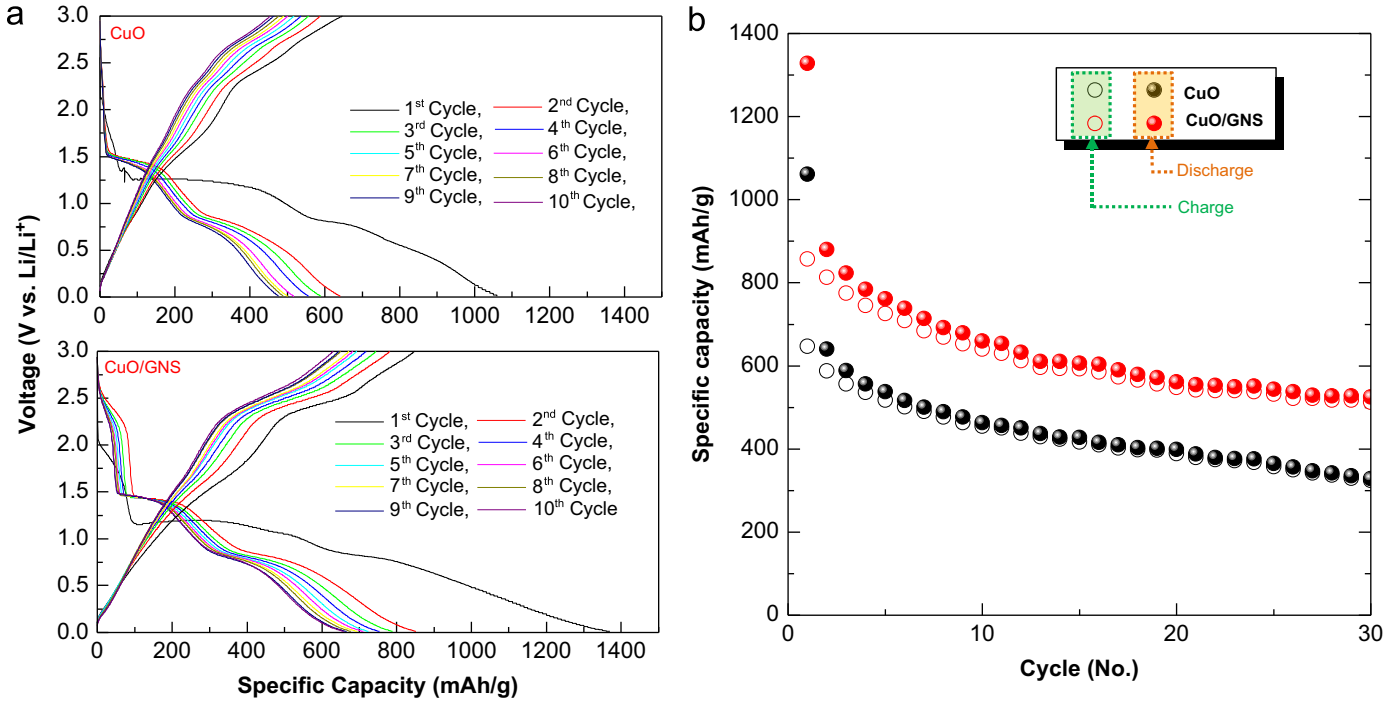

Fig. 4. (a) Voltage profile of CuO and CuO/GNS electrodes for the first 10 cycles and (b) cycle-capacity plots of CuO and CuO/GNS nanocomposite electrode (red circles: CuO/GNS, black circles: pure CuO). (For interpretation of the references to color in this figure legend, the reader is referred to the web version of this article.)

shown in Fig. 4b. The electrochemical performance of the CuO/GNS electrode was similar to that of pure CuO, but a relatively a large reversible capacity and cycle stability were observed in the case of the former. In the first cycle, the CuO/GNS composite showed a very large capacity of about 1400 mA h g^{-1}, although the theoretical capacity was only about 600 mA h g^{-1}. The reversible capacity of pure CuO was about 1050 mA h g^{-1} in the first discharge cycle; this value reduced to 650 mA h g^{-1}, which was higher than the theoretical capacity, after 10 cycles. This initial large capacity was due to the formation of a solid-electrolyte interface layer during the first discharge or the reduction of surface impurities and adsorbed hydrates. In particular, since the CuO/GNS electrode has a larger surface area than does the pure CuO electrode (an active material/electrolyte interface is possible in the former case), undesirable side reactions may occur. Generally, these side reactions lead to irreversible capacity in the initial discharge cycles. After 30 cycles, the CuO/GNS and CuO electrodes showed capacities of more than 500 mA h g^{-1} and about 300 mA h g^{-1}, respectively.

The capacity of the composite electrode was 1.5 times higher than that of the pure CuO electrode. Such significantly enhanced cycle performance of the CuO/GNS composite could provide valuable information on the role of the GNS in the composite. The synthesis procedure

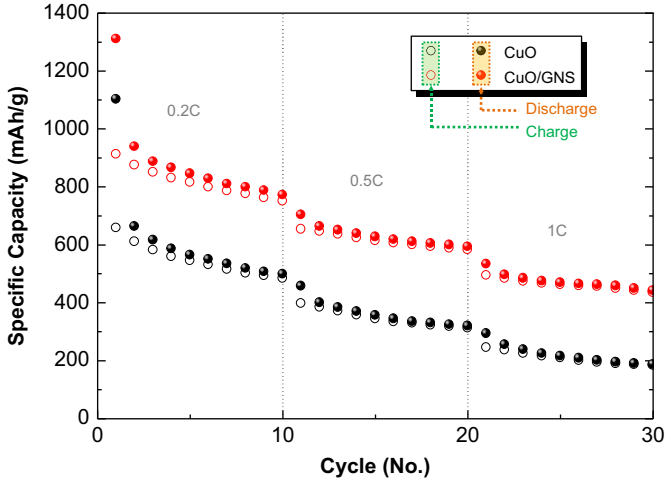

Fig. 5. Cycle-capacity plots of CuO (black circles) and CuO/GNS (red circles) at various current rates (0.2C→0.5C→1C). (For interpretation of the references to color in this figure legend, the reader is referred to the web version of this article.)

after the dispersion of the GNS was identical to that in the case of pure CuO. The nanoparticles synthesized by both methods had almost the same size, crystal structure, and shape. When fabricating composites of GNS with other materials, the high electrical conductivity of the former would enhance the reaction kinetics of the active material by enabling efficient electron supply between the current collectors. Pre-dispersion of the GNSs in solution allows for uniform mixing of the nanosheets with amorphous carbon (conducting additive) and helps in preventing problems that are normally encountered during mechanical mixing. Thus, the GNS affords an efficient conduction pathway in the composite and acts a self-agglomeration inhibitor.

To investigate the electron transportation route in the CuO/GNS composite, the rate capability of GNS was determined by galvanostatic cycling at various current rates. The cycle-capacity plots of CuO and the CuO/GNS composite samples tested at various current rates of 0.2–1C (on the basis of the theoretical capacity) are shown in Fig. 5. The CuO/GNS composite had better rate capability than did pure CuO. At 1C ($\sim$600 mA g^{-1}), CuO/GNS showed a stabilized capacity of more than 400 mA h g^{-1}, which was twice that of the pure CuO. Thus, we concluded that the GNS plays an important role in the composite by affording a larger active surface area and an efficient electron conduction pathway.

4. Conclusions

In summary, we synthesized pine-nut-like CuO nanoparticles by a simple and facile solution-based reduction process. Furthermore, we synthesized a CuO/GNS nanocomposite by a similar method, using electrolytically exfoliated GNS, without employing any surfactant or complex procedure. The composite had a uniform morphology and showed good phase agreement; no agglomeration of CuO particles or any secondary phase was observed. The pine-nut-shaped CuO/GNS composite showed better electrochemical performance than did pure CuO, with good current rate capability and a reversible capacity of more than 400 mA h g^{-1} after 30 cycles.

Acknowledgement

This work was supported by the National Research Foundation of Korea (NRF) grant funded by the Korea Government (MEST) (No. 2011-0030745) and Ajou University research fellowship of 2011 (S-2011-G0001-00070).

References

[1] D.W. Kim, Y.D. Ko, J.G. Park, B.K. Kim, Formation of lithium-driven active/inactive nanocomposite electrodes based on $Ca_3Co_4O_9$ nanoplates, Angewandte Chemie International Edition 46 (2007) 6654–6657.
[2] P. Poizot, S. Laruelle, S. Grugeon, L. Dupont, J.M. Tarascon, Nano-sized transition-metal oxides as negative-electrode materials for lithium-ion batteries, Nature 407 (2000) 496–499.
[3] S. Grugeon, S. Laruelle, R. Herrera-Urbina, L. Dupont, P. Poizot, J.M. Tarascon, Particle size effects on the electrochemical performance of copper oxides toward lithium, Journal of the Electrochemical Society 148 (2001) A285–A292.
[4] X. Zhang, D. Zhang, X. Ni, H. Zheng, Optical and electrochemical properties of nanosized CuO via thermal decomposition of copper oxalate, Solid State Electronics 52 (2008) 245–248.
[5] S.D. Seo, Y.H. Jin, S.H. Lee, H.W. Shim, D.W. Kim, Low-temperature synthesis of CuO-interlaced nanodiscs for lithium ion battery electrodes, Nanoscale Research Letters 6 (2011) 397.
[6] M. Xu, F. Wang, B. Ding, X. Song, J. Fang, Electrochemical synthesis of leaf-like CuO mesocrystals and their lithium storage properties, RSC Advances 2 (2012) 2240–2243.
[7] F. Wang, W. Tao, M. Zhao, M. Xu, S. Yang, Z. Sun, L. Wang, X. Song, Controlled synthesis of uniform ultrafine CuO nanowires as anode material for lithium-ion batteries, Journal of Alloys and Compounds 509 (2011) 9798–9803.
[8] Q. Pan, K. Huang, S. Ni, F. Yang, S. Lin, D. He, Synthesis of sheaf-like CuO from aqueous solution and their application in lithium-ion batteries, Journal of Alloys and Compounds 484 (2009) 322–326.
[9] J.G. Kang, Y.D. Ko, J.G. Park, D.W. Kim, Origin of capacity fading in nano-sized Co_3O_4 electrodes: electrochemical impedance spectroscopy study, Nanoscale Research Letters 3 (2008) 390–394.
[10] G.H. Lee, J.G. Park, Y.M. Sung, K.Y. Chung, W.I. Cho, D.W. Kim, Enhanced cycling performance of an Fe^0/Fe_3O_4 nanocomposite electrode for lithium-ion batteries, Nanotechnology 20 (2009) 295205.
[11] P.L. Taberna, S. Mitra, P. Poizot, P. Simon, J.M. Tarascon, High rate capabilities Fe_3O_4-based Cu nano-architectured electrodes for lithium-ion battery applications, Nature Materials 5 (2006) 567–573.
[12] H.W. Shim, Y.H. Jin, S.D. Seo, S.H. Lee, D.W. Kim, Highly reversible lithium storage in bacillus subtilis-directed porous Co_3O_4 nanostructures, ACS Nano 5 (2011) 443–449.
[13] K.S. Park, S.D. Seo, Y.H. Jin, S.H. Lee, H.W. Shim, D.H. Lee, D.W. Kim, Synthesis of cuprous oxide nanocomposite electrodes by room-temperature chemical partial reduction, Dalton Transactions 40 (2011) 9498–9530.
[14] Z.S. Wu, W. Ren, L. Wen, L. Gao, J. Zhao, Z. Chem, G. Zhou, F. Li, H.M. Cheng, Graphene anchored with Co_3O_4 nanoparticles as anode of lithium ion batteries with enhanced reversible capacity and cyclic performance, ACS Nano 4 (2010) 3187–3194.
[15] H. Wang, L.F. Cui, Y. Yang, H.S. Casalongue, J.T. Robinson, Y. Liang, Y. Cui, H. Dai, Mn_3O_4-graphene hybrid as a high-capacity

anode material for lithium ion batteries, Journal of the American Chemical Society 132 (2012) 13978–13980.
[16] Y.H. Jin, S.D. Seo, H.W. Shim, K.S. Park, D.W. Kim, Synthesis of core/shell spinel ferrite/carbon nanoparticles with enhanced cycling stability for lithium ion battery anodes, Nanotechnology 23 (2012) 125402.
[17] Y.J. Mai, X.L. Wang, J.Y. Xiang, Y.Q. Qiao, D. Zhang, C.D. Gu, J.P. Tu, CuO/graphene composite as anode materials for lithium-ion batteries, Electrochimica Acta 56 (2011) 2306–2311.
[18] J. Zhou, L. Ma, H. Song, B. Wu, X. Chen, Durable high-rate performance of CuO hollow nanoparticles/graphene-nanosheet composite anode material for lithium-ion batteries, Electrochemistry Communications 13 (2011) 1357–1360.
[19] B. Wang, X.L. Wu, C.Y. Shu, Y.G. Guo, C.R. Wang, Synthesis of CuO/graphene nanocomposite as a high-performance anode material for lithium-ion batteries, Journal of Materials Chemistry 20 (2010) 10661–10664.
[20] S.H. Lee, S.D. Seo, Y.H. Jin, H.W. Shim, D.W. Kim, A graphite foil electrode covered with electrochemically exfoliated graphene nanosheets, Electrochemistry Communications 12 (2010) 1419–1422.
[21] Y.H. Jin, S.H. Lee, H.W. Shim, K.H. Ko, D.W. Kim, Tailoring high-surface-area nanocrystalline TiO_2 polymorphs for high-power Li ion battery electrodes, Electrochimica Acta 55 (2010) 7315–7321.
[22] C. Wu, P. Yin, X. Zhu, C. Ouyang, Y. Xie, Synthesis of hematite (α-Fe_2O_3) nanorods: diameter-size and shape effects on their applications in magnetism, lithium ion battery, and gas sensors, Journal of Physical Chemistry B 110 (2006) 17806–17812.
[23] Y. Cudennec, A. Lecerf, The transformation of $Cu(OH)_2$ into CuO, revisited, Solid State Sciences 5 (2003) 1471–1474.
[24] J.Y. Xiang, J.P. Tu, Y. Zhou, X.L. Wang, S.J. Shi, Self-assembled synthesis of hierarchical nanostructured CuO with various morphologies and their application as anodes for lithium ion batteries, Journal of Power Sources 195 (2010) 313–319.
[25] S.D. Seo, I.S. Hwang, S.H. Lee, H.W. Shim, D.W. Kim, 1D/2D carbon nanotube/graphene nanosheet composite anodes fabricated using electrophoretic assembly, Ceramics International 38 (2012) 3017–3021.
[26] P. Novak, CuO cathode in lithium cells-II. Reduction mechanism of CuO, Electrochimica Acta 30 (1985) 1687–1692.
[27] S. Laruelle, S. Grugeon, P. Poizot, M. Dolle, L. Dupont, J.M. Tarascon, On the origin of the extra electrochemical capacity displayed by MO/Li cells at low potential, Journal of the Electrochemical Society 149 (2002) A627–A634.